THE JOURNAL OF PHYSICAL CHEMISTRY Letters

Letter

pubs.acs.org/JPCL

Piezotronic-Enhanced Photoelectrochemical Reactions in $Ni(OH)_2$-Decorated ZnO Photoanodes

Hongxia Li,[†,‡,§] Yanhao Yu,[†,§] Matthew B. Starr,[†] Zhaodong Li,[†] and Xudong Wang*[,†]

[†]Department of Materials Science and Engineering, University of Wisconsin-Madison, Madison, Wisconsin 53706, United States

[‡]College of Materials and Environmental Engineering, Hangzhou Dianzi University, Hangzhou, 310018, People's Republic of China

Supporting Information

ABSTRACT: Controlling the interface electronic band structure in heterostructures is essential for developing highly efficient photoelectrochemical (PEC) photoanodes. Here, we presented an enhanced oxygen evolution reaction (OER) by introducing the piezotronics concept, i.e., piezoelectric polarization (P_{pz})-induced band engineering. In a $Ni(OH)_2$-decorated ZnO photoanode system, appreciably improved photocurrent density of sulfite (SO_3^{2-}) and hydroxyl (OH^-) oxidation reactions were obtained by physically deflecting the photoanode. Both theoretical and experimental results suggested that the performance enhancement was a result of the piezoelectric P_{pz}-endowed enlargement of the built-in electric field at the $ZnO/Ni(OH)_2$ interface, which could drive an additional amount of photoexcited charges from ZnO toward the interface for OER. This strategy demonstrates a new route for improving the performance of inexpensive catalysts-based solar-to-fuel production.

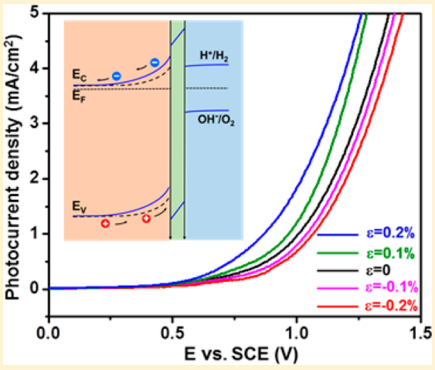

Photoelectrochemical (PEC) water splitting is a promising strategy for converting solar energy to chemical fuels.[1] In traditional photovoltaic (PV) devices, a high-quality p−n junction is required for efficient photoexcited charge separation. Many factors complicate the preparation of high-quality p−n junctions, including proper alignment of band structures, high crystal quality, and precise dopant control. Compared to PV devices, a PEC system is relatively simpler, where the energy discontinuity at the semiconductor/electrolyte interface provides necessary driving force to separate photoexcited charges.[2,3] In a typical PEC water splitting process, photoexcited holes are involved in oxidation reactions at the photoanode, converting hydroxyl (OH^-) to oxygen gas (O_2). At the photocathode, photoexcited electrons take part in reduction reactions, where protons in hydronium molecules (H_3O^+) are reduced to hydrogen gas (H_2). These oxidation and reduction reactions are referred to as the oxygen evolution reaction (OER) and hydrogen evolution reaction (HER), respectively. Thermodynamically, the minimum energy required for splitting H_2O into H_2 and $1/2O_2$ is 1.23 eV. In addition to the thermodynamic limit, additional activation energy is needed to overcome the kinetic barrier and increase the rate of electrochemical reaction. To minimize the requirement of activation energy, OER and HER catalysts are frequently applied to the surface of semiconductor photoelectrodes. Noble metals such as platinum and iridium have shown excellent catalytic performance in both OER[4,5] and HER[6,7] processes. However, large-scale industrial application of these catalysts has been severely limited by their high cost. Recently, pure transition-metals and transition-metal oxides and hydroxides have emerged as promising low-cost catalysts, especially for OER.[8−18] Unlike the noble metal catalysts, these oxides and hydroxides are predominantly insulators. Introducing an insulating catalyst between the semiconductor photoelectrode and electrolyte will induce a significant drop of the total potential (defined by the initial Fermi level difference between semiconductor and electrolyte, denoted as φ_0) in the catalyst layer, and thus reduce the built-in potential (φ_{bi}) and depletion width (L_d) in the semiconductor. The reduced φ_{bi} and L_d impairs the efficiency of photoexcited charge separation and holes injection. To alleviate these drawbacks of applying an insulating catalyst layer, additional consideration should be given to enhancing the semiconductor/electrocatalyst interfacial electronic structure and properties.

The piezotronic effect is a recently proposed principle for locally engineering the band structures of heterojunctions using piezoelectric polarization (P_{pz}).[19−22] P_{pz} can be generated by mechanically straining a piezoelectric material and considerably influences the free charge distribution and the band structure at the piezoelectric/semiconductor interface. Applying P_{pz} to control the charge transport properties of semiconductor devices has been employed in gating nanowire-based field-effect transistors (FET),[19,21] manipulating electro- or photoluminescence,[22−25] optimizing photovoltaics performance,[26] and facilitating electrochemical reactions.[27−29] The performance gains induced by P_{pz} were found to be stable since P_{pz} can be maintained durably upon constant deformation.[22,28] Here, we studied the application of the piezotronic concept to

Received: July 24, 2015
Accepted: August 16, 2015
Published: August 16, 2015

DOI: 10.1021/acs.jpclett.5b01598
J. Phys. Chem. Lett. 2015, 6, 3410−3416

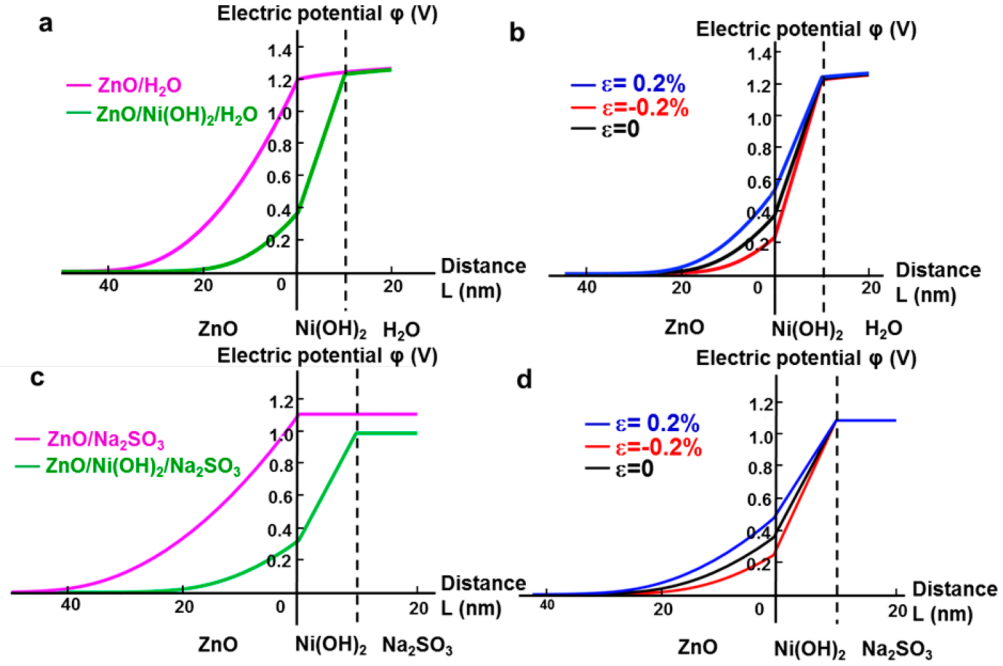

Figure 1. Calculated electric potential (φ) distribution across the ZnO/Ni(OH)$_2$/H$_2$O and ZnO/Ni(OH)$_2$/Na$_2$SO$_3$ heterojunctions. (a) φ distribution of ZnO/H$_2$O with (green) and without (magenta) Ni(OH)$_2$ catalyst layer. Significantly reduced band bending of ZnO can be observed after inserting Ni(OH)$_2$. (b) φ distribution of ZnO/Ni(OH)$_2$/H$_2$O under different strain conditions (denote strain as ε). Positive and negative strain can increase and decrease the depletion of ZnO, respectively. The influence of P_{pz} was dramatically pronounced after adding Ni(OH)$_2$. (c) φ distribution of ZnO/Na$_2$SO$_3$ with (green) and without (magenta) Ni(OH)$_2$ catalyst layer. Ni(OH)$_2$ decreased the band bending of ZnO. (d) φ distribution of ZnO/Ni(OH)$_2$/Na$_2$SO$_3$ under different strain conditions, showing that positive and negative strain can increase and decrease the depletion of ZnO, respectively.

enhancing the performance of inexpensive catalysts in OER. In a ZnO/Ni(OH)$_2$-based photoanode system, P_{pz} was introduced to increase the electric field strength in the vicinity of the semiconductor/electrolyte heterojunction, expanding the depletion length, and thus driving an additional amount of photoexcited charges toward the interface for the OER. By physically deflecting a laminate ZnO/Ni(OH)$_2$ photoanode, appreciably improved photocurrent density (J_{ph}) of sulfite (SO_3^{2-}) and OH^- oxidation reactions were obtained. Both theoretical and experimental results suggested that the performance gain was a result of the piezotronic-induced enlargement of the built-in electric field at the ZnO/Ni(OH)$_2$ interface. This strategy demonstrates a new route for improving the performance of OER catalysts for achieving efficient PEC water splitting.

To investigate the influence of P_{pz} on OER performance, the potential distribution across the ZnO/Ni(OH)$_2$/H$_2$O heterojunction was first calculated numerically (see Supporting Information for calculating details, S3). As shown in Figure 1a, for a photoanode held at 1 V vs SCE, without Ni(OH)$_2$ (i.e., a ZnO/H$_2$O junction), ZnO and H$_2$O share 80.9% and 19.1% of φ_0, respectively. After adding a 10 nm-thick Ni(OH)$_2$ layer between the ZnO and H$_2$O, the majority (58%) of φ_0 is dropped within the insulating Ni(OH)$_2$. The electric potential shared by ZnO and H$_2$O decreased to 25% and 17%, respectively. Meanwhile, L_d of ZnO was reduced from 37.6 to 20.3 nm. This calculation suggests that an insulating Ni(OH)$_2$ layer between the ZnO and H$_2$O will cause a deterioration of φ_{bi} and L_d in the photoactive ZnO film.

We next introduced strain to the model to investigate the influence of P_{pz}. Figure S1 presents the potential distribution of the ZnO/H$_2$O junction, under uniform positive (tensile) and negative (compressive) strain, perpendicular to the ZnO/H$_2$O interface, when a bias of 1 V vs SCE applied to the ZnO anode. It was found that when the ZnO layer is strained, P_{pz} has little effect on the band positions at the interface, changing the junction potential by less than 21 mV. When an insulating Ni(OH)$_2$ layer with low dielectric constant (~3.4)[30] is introduced between ZnO and H$_2$O (Figure 1b), the impact of the strain-induced P_{pz} on the energetics of ZnO is intensified. The insulating Ni(OH)$_2$ layer increases the energetic penalty of redistributing charge in H$_2$O relative to redistributing charge in ZnO, thus ZnO provides the majority of charge redistribution and compensation necessary to balance P_{pz}. Under these conditions, a tensile strain of 0.2% uniformly applied to ZnO, perpendicular to the junction, increased the φ_{bi} and L_d of ZnO from 0.37 to 0.53 eV and 20.3 to 24.6 nm, respectively. A compressive strain of −0.2% reduced the φ_{bi} and L_d to 0.23 eV and 15.7 nm, respectively. As shown in Figure S2, the influence of P_{pz} on the φ_{bi} and L_d of ZnO could be amplified by increasing Ni(OH)$_2$ thickness.

The effect of increasing the electrolyte concentration on the expression of P_{pz} was then investigated. Figure 1c shows the electrical potential profiles for a ZnO/Na$_2$SO$_3$ solution (1 M in H$_2$O) junction with and without a 10 nm-thick insulating Ni(OH)$_2$ layer. Without the Ni(OH)$_2$, the majority (<99.9%) of electrical potential change across the interface is within ZnO. After adding a 10 nm-thick Ni(OH)$_2$ layer between the ZnO and Na$_2$SO$_3$ solution, the majority (67.1%) of φ_0 is found to drop within the insulating Ni(OH)$_2$. The electric potential shared by ZnO and Na$_2$SO$_3$ solution decreased to 32.8% and 0.05%, respectively. Meanwhile, L_d of ZnO was reduced from 44.3 to 23.5 nm. Applying strain directly to a ZnO/Na$_2$SO$_3$ junction was found to have no effect (<1 mV) on the potential

DOI: 10.1021/acs.jpclett.5b01598
J. Phys. Chem. Lett. 2015, 6, 3410−3416

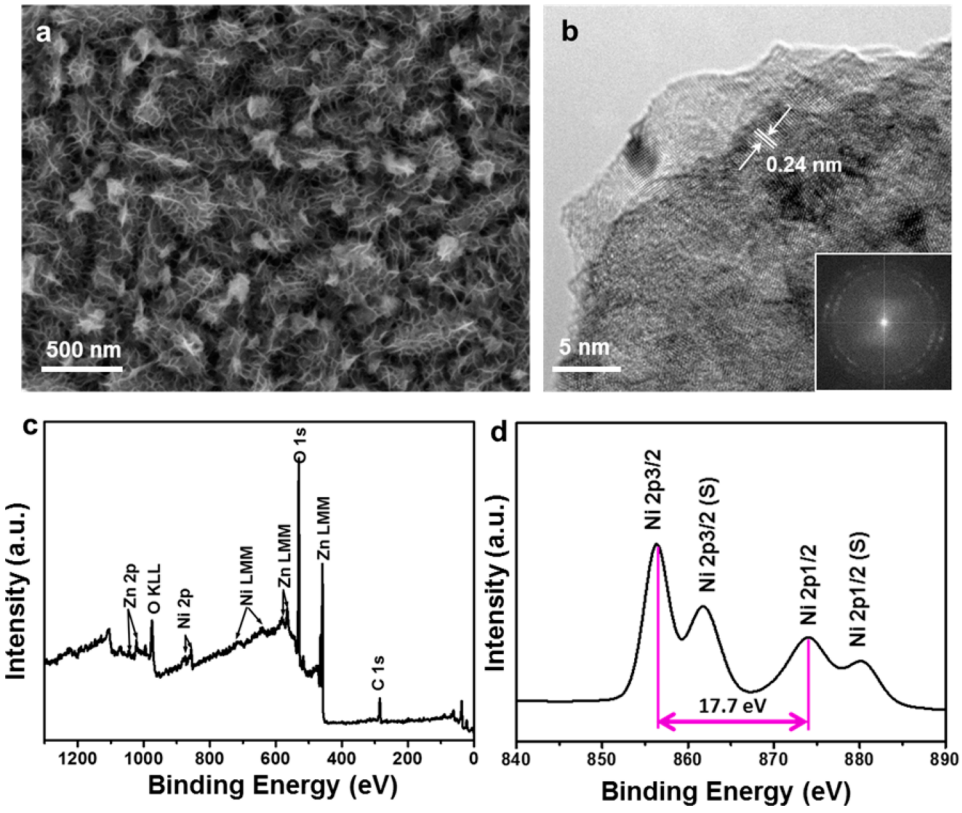

Figure 2. Structure and elemental characterizations of a ZnO/$Ni(OH)_2$ heterostructure. (a) SEM image of electrodeposited $Ni(OH)_2$ on ZnO film. A sheet-like $Ni(OH)_2$ layer with a wrinkled surface was uniformly covered on the entire ZnO surface. (b) TEM observation of an individual $Ni(OH)_2$ sheet. The inset is the corresponding FFT, which reveals the polycrystalline feature of $Ni(OH)_2$. (c) Full-range XPS spectrum acquired from a ZnO/$Ni(OH)_2$ heterojunction. (d) Ni 2p scan for ZnO/$Ni(OH)_2$ heterostructure. The spin-energy separation of 17.7 eV between Ni 2p3/2 and Ni 2p1/2 peaks verified the $Ni(OH)_2$ composition.

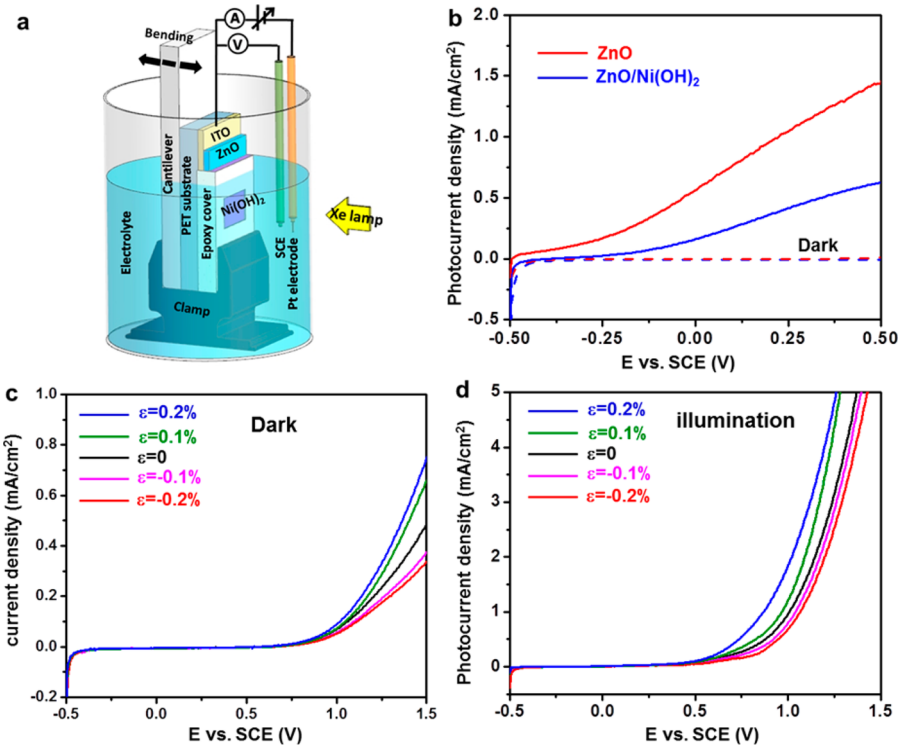

Figure 3. P_{pz} enhanced sulfite oxidation based on ZnO/$Ni(OH)_2$ photoanode. (a) Schematic drawing of experimental setup for investigating the influence of P_{pz} on sulfite oxidation and OER. (b) J_{ph}–V curves of ZnO (red) and ZnO/$Ni(OH)_2$ (blue) photoanode for sulfite oxidation. (c,d) J–V characterizations of ZnO/$Ni(OH)_2$ with various strains under dark (c) and 150 W Xe lamp illumination (d).

DOI: 10.1021/acs.jpclett.5b01598
J. Phys. Chem. Lett. 2015, 6, 3410–3416

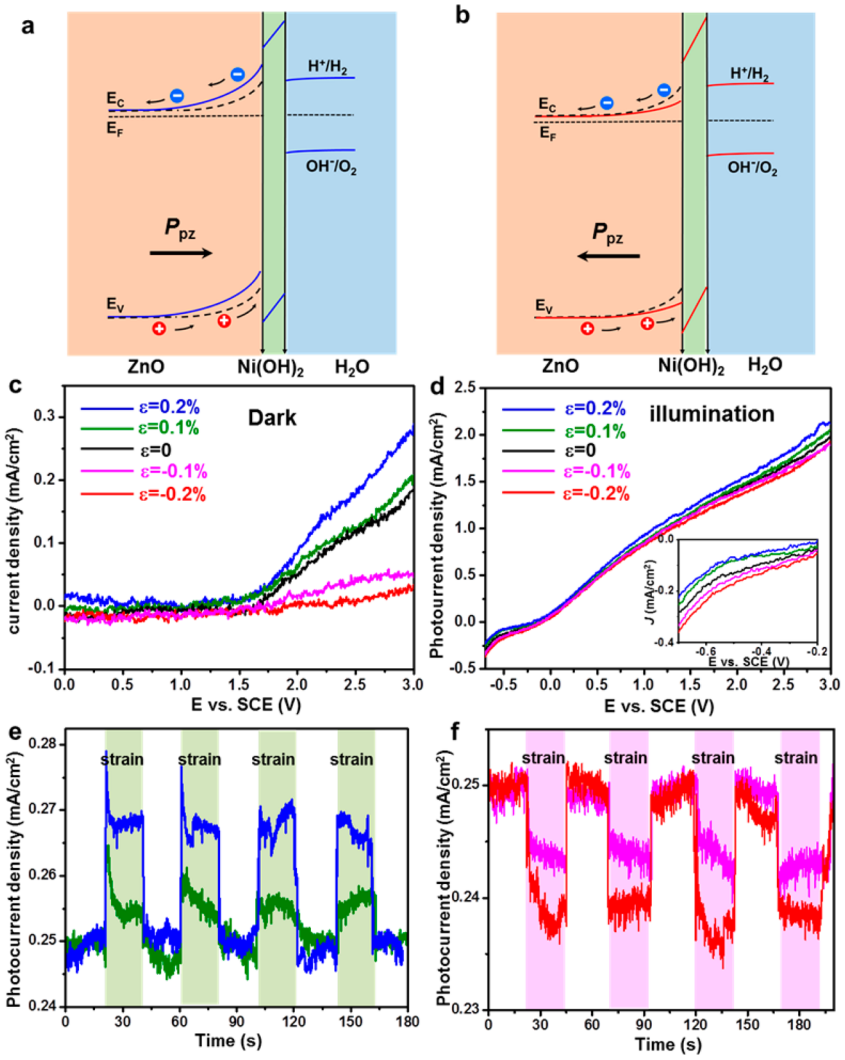

Figure 4. Strain-related OER performance of $ZnO/Ni(OH)_2$ photoanode. (a,b) Band diagram of $ZnO/Ni(OH)_2$/DI-H_2O heterojunction when it was subjected to a positive (a) and negative (b) strain. The band bending scale was referred to the calculated potential distribution in Figure 1b. (c,d) $J-V$ curves of $ZnO/Ni(OH)_2$ photoanode for OER under different strain conditions in dark circumstance (c) and 150 W Xe lamp illumination (d). (e,f) J_{ph} of $ZnO/Ni(OH)_2$ photoanode under periodic positive (e) 0.1% (green) and 0.2% (blue) strains, and negative (f) 0.1% (magenta) and 0.2% (red) strains at a constant bias of 1 V versus SCE. The positive and negative strained regions are marked with light green and pink, respectively. J_{ph} were collected under 150 W Xe lamp illumination.

distribution (Figure S3) because P_{pz} is completely screened by charge redistribution (stern layer formation) in the 1 M Na_2SO_3 solution. Applying an insulating $Ni(OH)_2$ layer between ZnO and Na_2SO_3 revives the energy penalty of screening P_{pz} via charge redistribution in the solution phase (Figure 1d). For the $ZnO/Ni(OH)_2/Na_2SO_3$ interface, a tensile strain of 0.2% uniformly applied to the ZnO, perpendicular to the junction, increased the φ_{bi} and L_d of ZnO from 0.49 to 0.65 eV and 23.5 to 37.4 nm, respectively. A compressive strain of −0.2% reduced the φ_{bi} and L_d to 0.34 eV and 19.3 nm, respectively. Under proper conditions (e.g., an $Ni(OH)_2$ layer and positive strain), both the increased electric field strength at the ZnO interface and the greater depth of the electric field into the bulk of ZnO are expected to contribute to an increase in the total number of photoexcited charges that are successfully separated and driven toward the water interface, resulting in higher J_{ph} and OER performance.

The calculated piezotronic enhancement was then tested in a strained PEC water splitting system. The piezo-photoanode comprised three layers: a flexible indium tin oxide (ITO)-coated polyethylene terephthalate (PET) substrate, a radio frequency sputtered ZnO film, and a layer of electrodeposited $Ni(OH)_2$ catalyst. The morphology of the electrodeposited $Ni(OH)_2$ film was characterized using scanning electron microscopy (SEM) as shown in Figure 2a. The rough $Ni(OH)_2$ layer had a sheet-like structure with wrinkled surface features and a uniform coverage over the ZnO photoanode. Individual $Ni(OH)_2$ sheets were semitransparent under transmission electron microscopy (TEM) (Figure S4), indicating a small film thickness. A high-resolution TEM image (Figure 2b) and its corresponding fast Fourier transform (FFT; inset of Figure 2b) revealed that the $Ni(OH)_2$ film was polycrystalline. The lattice distance was measured to be 0.24 nm, agreeing well with the (011) plane of β-$Ni(OH)_2$.[31] Elemental characteristics of the $ZnO/Ni(OH)_2$ heterojunction were further studied by X-ray photoelectron spectroscopy (XPS). The full XPS spectrum (Figure 2c) showed good agreement with all the elements expected in a ZnO and $Ni(OH)_2$ sample. The peak centered at 1022.1 eV is the signature peak of Zn^{2+} in ZnO, corresponding to the Zn 2p3/2 core level (Figure S5).[16,32,33] Its symmetrical

DOI: 10.1021/acs.jpclett.5b01598
J. Phys. Chem. Lett. 2015, 6, 3410−3416

shape indicates a perfect stoichiometry of the sputtering ZnO film. The two major peaks with binding energies of 856.3 and 874 eV, and their associating satellite peaks located at higher binding energies, were attributed to the Ni 2p3/2 and Ni 2p1/2 binding energies, respectively (Figure 2d). The spin-energy separation of 17.7 eV between the Ni 2p3/2 and Ni 2p1/2 peaks corroborated the $Ni(OH)_2$ composition.[34,35]

The influence of P_{pz} on the PEC performance was first studied in 1 M Na_2SO_3 electrolyte, which acted as a photoexcited hole scavenger.[13] Although the fundamental principles are the same, sulfite (SO_3^{2-}) oxidation is thermodynamically and kinetically more favorable compared to OER. SO_3^{2-}oxidation is thus a model system for investigating the effect of P_{pz} on photoexcited charge separation at the ZnO/$Ni(OH)_2$ interface. The device and measurement setup are schematically shown in Figure 3a. This PEC cell has a layered structure of PET/ITO/ZnO/$Ni(OH)_2$. The working area was confined to ∼0.1 cm^2 by epoxy coating. The entire device was attached to a poly(methyl methacrylate) (PMMA) cantilever, which can be deformed to produce different strains to the photoanode. A three electrode configuration was adopted for PEC measurement with platinum wire and saturated calomel electrode (SCE) as the counter and reference electrode, respectively. As shown on Figure 3b, upon 150 W Xe lamp illumination, the J_{ph} of a pristine ZnO photoanode, exposed directly to the Na_2SO_3 solution, reached ∼1.4 mA cm^{-2} at a bias of 0.5 V versus SCE. This J_{ph} is 2.8 times larger than that of ZnO/$Ni(OH)_2$/Na_2SO_3 heterojunction (∼0.5 mA cm^{-2} at bias of 0.5 V versus SCE) under the same conditions. According to the calculated potential distribution of ZnO/Na_2SO_3 and ZnO/$Ni(OH)_2$/Na_2SO_3, the pronounced decline of J_{ph} after adding $Ni(OH)_2$ to the surface of ZnO is attributed to the significant reduction of φ_{bi} and L_d in the ZnO (see Figure 1c), thus reducing the efficiency of photoexcited charge separation and reducing the concentration of charges at the interface. Trapping states (recombination centers) at the ZnO/$Ni(OH)_2$ interface and the high electrical resistance of $Ni(OH)_2$ may also contribute to the decreased J_{ph}.[13] In order to reduce the influence from interface trapping states, a planar configuration, as opposed to a nanostructed heterojunction, was adopted.[13] A small $Ni(OH)_2$ film thickness was maintained to minimize the resistance losses.

Calculations suggested that the unfavorable change in interfacial band structure caused by adding a $Ni(OH)_2$ film onto the ZnO surface (Figure 1c) can be compensated by the P_{pz} created by straining the ZnO (Figure 1d). Figure 3c shows the current density-potential (J–V) curve of the ZnO/$Ni(OH)_2$/Na_2SO_3 PEC under different straining conditions without light illumination. In general, positive strain increased J and negative strain decreased J, in agreement with predictions made from calculation. Specifically, 0.1% and 0.2% strain increased J from 0.482 mA cm^{-2} to 0.654 mA cm^{-2} and 0.740 mA cm^{-2} at bias of 1.5 V versus SCE, corresponding to an improvement of ∼36% and ∼85%, respectively. Applying −0.1% and −0.2% strain decreased J from 0.482 mA cm^{-2} to 0.374 mA cm^{-2} and 0.338 mA cm^{-2}, corresponding to an reduction of ∼22% and ∼30%, respectively. Under Xe lamp illumination, the absolute values of J_{ph} are significantly increased (Figure 3d). At a bias range of 0.5–1.5 V versus SCE, SO_3^{2-} oxidation occurred, and J_{ph} responded to the applied strain in the same manner as in the dark condition, where an increase and decrease of J_{ph} are clearly identified upon positive and negative strains, respectively. These mechanical strain-induced variations to J and J_{ph} are believed to be the consequence of altered electron–hole separation and holes injection efficiency, reinforcing the conclusion that P_{pz} is capable of significantly manipulating the interfacial band structure of the ZnO/$Ni(OH)_2$ heterojunction.

To reveal the influence of P_{pz} on the OER, the Na_2SO_3 electrolyte was replaced with deionized (DI)-H_2O. For a typical ZnO/$Ni(OH)_2$ photoanode, the driving force for separating photogenerated charges originates in the energy difference between the Femi level of ZnO and electrolyte solution. With the addition of mechanical strain as a variable, P_{pz} is expected to augment the driving force for electron transfer reactions at the interface. Figure 4a,b shows the band diagram derived from calculation for the ZnO/$Ni(OH)_2$/DI-H_2O heterojunction under positive and negative strains, respectively (Figure 1b). Under positive strain, the ZnO film will generate a P_{pz} with a direction pointing toward the ZnO/$Ni(OH)_2$ interface.[26] Mobile charges in the ZnO, $Ni(OH)_2$ and DI-H_2O will redistribute to screen the strain-induced P_{pz}. The low conductivity and low dielectric constant $Ni(OH)_2$ film increases the energetic penalty of screening the P_{pz} via charge redistribution in the DI-H_2O as compared to the ZnO. As charge redistribution takes place in the ZnO to screen P_{pz}, φ_{bi} and L_d in the ZnO increase (Figure 4a). This enhanced band bending is expected to speed up the efficiency of photoexcited charge separation, accelerating the rate of holes injection into $Ni(OH)_2$ and therefore increasing the J_{ph}. Conversely, negative stain will induce an opposite P_{pz}, shallowing the depletion region in ZnO and reducing J_{ph} (Figure 4b).

To investigate this effect, the PEC performance of the ZnO/$Ni(OH)_2$ anode was measured in DI-H_2O under different straining conditions. Without applying any strain or light, the current remained at a low level between a bias of −0.5 and 1.5 V versus SCE (Figure 4c). When the bias was greater than 1.5 V, the OER began. Similar to SO_3^{2-} oxidation, the largest and smallest J were measured with 0.2% and −0.2% strain, respectively, indicating that P_{pz} has an influence on hole-injection capability under a constant bias. Both in the dark and when illuminated by a Xe lamp (Figure 4d), J had an approximately linear relationship to both potential and strain. This linear response of both J and J_{ph} to the applied potential is likely because the OER in DI H_2O is both extremely kinetically and diffusion limited. These factors are not strongly influenced by the energetic landscape on the electrode-side of the junction, and thus the effect of strain on J and J_{ph} remained small. It is useful to compare J and J_{ph} as a function of strain, where strain had a greater effect on J than on J_{ph}. This phenomenon was also observed in P_{pz}-modulated PVs and was known as a consequence of photoexcited charges screening the P_{pz}.[26] Photoexcited charges are expected to most prominently screen P_{pz} when the charges do not have an efficient electron source and sink to reduce their concentration in the vicinity of the interface. This situation is exactly what was encountered under our DI-H_2O experimental condition. A magnified J_{ph}–V curve in the negative bias region (inset of Figure 4d) shows a reversal of the strain-related current deviation trend as compared to the positive bias region (i.e., positive strain reduced J_{ph}). This observation is evidence that the observed current variation is a result of band engineering rather than piezo-induced resistance change,[19] which would exhibit a linear J_{ph}–V curve.

In order to further investigate the effect of P_{pz} on PEC performance, J_{ph} was characterized at a fixed external bias of 1 V versus SCE as a function of pulsed strain. Figure 4e,f present

DOI: 10.1021/acs.jpclett.5b01598
J. Phys. Chem. Lett. 2015, 6, 3410–3416

the J_{ph}−strain curves measured when strain was periodically applied to the ZnO/$Ni(OH)_2$ heterojunction. In general, J_{ph} exhibited a quick response to the strain. Under a tensile strain of 0.1% and 0.2%, J_{ph} increased from 0.249 mA cm^{-2} to 0.256 mA cm^{-2} and 0.268 mA cm^{-2}, respectively, demonstrating an enhanced OER activity under a constant bias but increased tensile strain. When subjected to a compressive strain of −0.1% and −0.2%, J_{ph} decreased from 0.249 mA cm^{-2} to 0.244 mA cm^{-2} and 0.239 mA cm^{-2}, respectively. The capacitive current spikes in Figure 4e, which appear immediately following the straining events, are indicative of the charge redistribution that takes place in ZnO immediately after the formation of P_{pz}.[28] These J_{ph}−strain characterizations are further evidence that P_{pz} is an effective approach to control the OER performance of $Ni(OH)_2$-decorated ZnO photoandes.

In summary, we report a novel strategy for manipulating the interfacial band structure of a ZnO/$Ni(OH)_2$ heterojunction using strain induced P_{pz}. Electrical potential distributions calculated for ZnO/$Ni(OH)_2$ heterojunctions indicate that P_{pz} is able to largely increase the φ_{bi} and L_d of ZnO at the ZnO/$Ni(OH)_2$ interface, improving the PEC performance. Experimentally, tensile strain of sputtered ZnO films increased both J and J_{ph} for sulfite and water oxidation reactions. These enhancements were attributed to the increased depth of electric field into the bulk of the ZnO and increased strength of the interfacial electric field, both contributing to an increased efficiency of photoexcited charge separation in ZnO. These results have shown the promise of using the piezotronic effect to improve the performance of OER catalysts on semiconductor photoelectrodes. Compared with other delicate band-engineering approaches, such as tuning the doping density of semiconductors and integrating high-quality ferroelectrics, this piezotronic strategy can be easily handed and precisely controlled. Further enhancement of PEC performance can be expected from optimizing the quality, conductivity, and piezoelectric property of the photoactive and piezoelectric material, as well as the thickness and quality of the insulating catalytic layer.

■ ASSOCIATED CONTENT

Supporting Information

Experimental details, calculation details of electric potential profile, additional electric potential distribution, TEM and XPS characterization. The Supporting Information is available free of charge on the ACS Publications website at DOI: 10.1021/acs.jpclett.5b01598.

(PDF)

■ AUTHOR INFORMATION

Corresponding Author

*E-mail: xudong.wang@wisc.edu.

Author Contributions

§These authors contributed equally.

Notes

The authors declare no competing financial interest.

■ ACKNOWLEDGMENTS

This work is supported by National Science Foundation under Award # CMMI-1148919 and Air Force Office of Scientific Research (AFOSR) under Award # FA9550-13-1-0168. H.L. thanks the China Scholarship Council for financial support.

■ REFERENCES

(1) Fujishima, A.; Honda, K. Electrochemical Photolysis of Water at a Semiconductor Electrode. *Nature* **1972**, *238*, 37−38.

(2) Walter, M. G.; Warren, E. L.; McKone, J. R.; Boettcher, S. W.; Mi, Q.; Santori, E. A.; Lewis, N. S. Solar Water Splitting Cells. *Chem. Rev.* **2010**, *110*, 6446−6473.

(3) Wang, X.; Li, Z.; Shi, J.; Yu, Y. One-Dimensional Titanium Dioxide Nanomaterials: Nanowires, Nanorods, and Nanobelts. *Chem. Rev.* **2014**, *114*, 9346−9384.

(4) Dasgupta, N. P.; Liu, C.; Andrews, S.; Prinz, F. B.; Yang, P. Atomic Layer Deposition of Platinum Catalysts on Nanowire Surfaces for Photoelectrochemical Water Reduction. *J. Am. Chem. Soc.* **2013**, *135*, 12932−12935.

(5) Chen, Y. W.; Prange, J. D.; Duhnen, S.; Park, Y.; Gunji, M.; Chidsey, C. E.; McIntyre, P. C. Atomic Layer-Deposited Tunnel Oxide Stabilizes Silicon Photoanodes for Water Oxidation. *Nat. Mater.* **2011**, *10*, 539−544.

(6) Esposito, D. V.; Levin, I.; Moffat, T. P.; Talin, A. A. H_2 Evolution at Si-Based Metal-Insulator-Semiconductor Photoelectrodes Enhanced By Inversion Channel Charge Collection and H Spillover. *Nat. Mater.* **2013**, *12*, 562−568.

(7) Ji, L.; McDaniel, M. D.; Wang, S.; Posadas, A. B.; Li, X.; Huang, H.; Lee, J. C.; Demkov, A. A.; Bard, A. J.; Ekerdt, J. G.; et al. A Silicon-Based Photocathode for Water Reduction with an Epitaxial $SrTiO_3$ Protection Layer and a Nanostructured Catalyst. *Nat. Nanotechnol.* **2015**, *10*, 84−90.

(8) Han, Z.; Qiu, F.; Eisenberg, R.; Holland, P. L.; Krauss, T. D. Robust Photogeneration of H_2 in Water Using Semiconductor Nanocrystals and a Nickel Catalyst. *Science* **2012**, *338*, 1321−1324.

(9) Gong, M.; Li, Y.; Wang, H.; Liang, Y.; Wu, J. Z.; Zhou, J.; Wang, J.; Regier, T.; Wei, F.; Dai, H. An Advanced Ni-Fe Layered Double Hydroxide Electrocatalyst for Water Oxidation. *J. Am. Chem. Soc.* **2013**, *135*, 8452−8455.

(10) Kenney, M. J.; Gong, M.; Li, Y.; Wu, J. Z.; Feng, J.; Lanza, M.; Dai, H. High-Performance Silicon Photoanodes Passivated with Ultrathin Nickel Films for Water Oxidation. *Science* **2013**, *342*, 836−840.

(11) Gao, M.; Sheng, W.; Zhuang, Z.; Fang, Q.; Gu, S.; Jiang, J.; Yan, Y. Efficient Water Oxidation Using Nanostructured α-Nickel-Hydroxide as an Electrocatalyst. *J. Am. Chem. Soc.* **2014**, *136*, 7077−7084.

(12) Hu, S.; Shaner, M. R.; Beardslee, J. A.; Lichterman, M.; Brunschwig, B. S.; Lewis, N. S. Amorphous TiO_2 Coatings Stabilize Si, GaAs, and GaP Photoanodes for Efficient Water Oxidation. *Science* **2014**, *344*, 1005−1009.

(13) Kim, T. W.; Choi, K. S. Nanoporous $BiVO_4$ Photoanodes with Dual-Layer Oxygen Evolution Catalysts for Solar Water Splitting. *Science* **2014**, *343*, 990−994.

(14) Lin, F.; Boettcher, S. W. Adaptive Semiconductor/Electrocatalyst Junctions in Water-Splitting Photoanodes. *Nat. Mater.* **2014**, *13*, 81−86.

(15) Luo, J.; Im, J. H.; Mayer, M. T.; Schreier, M.; Nazeeruddin, M. K.; Park, N. G.; Tilley, S. D.; Fan, H. J.; Gratzel, M. Water Photolysis at 12.3% Efficiency via Perovskite Photovoltaics and Earth-Abundant Catalysts. *Science* **2014**, *345*, 1593−1596.

(16) Mao, Y.; Yang, H.; Chen, J.; Chen, J.; Tong, Y.; Wang, X. Significant Performance Enhancement of ZnO Photoanodes from $Ni(OH)_2$ Electrocatalyst Nanosheets Overcoating. *Nano Energy* **2014**, *6*, 10−18.

(17) McCrory, C. C.; Jung, S.; Ferrer, I. M.; Chatman, S. M.; Peters, J. C.; Jaramillo, T. F. Benchmarking Hydrogen Evolving Reaction and Oxygen Evolving Reaction Electrocatalysts for Solar Water Splitting Devices. *J. Am. Chem. Soc.* **2015**, *137*, 4347−4357.

(18) Juodkazis, K.; Juodkazytė, J.; Vilkauskaitė, R.; Jasulaitienė, V. Nickel Surface Anodic Oxidation and Electrocatalysis of Oxygen Evolution. *J. Solid State Electrochem.* **2008**, *12*, 1469−1479.

(19) Wang, X.; Zhou, J.; Song, J.; Liu, J.; Xu, N.; Wang, Z. L. Piezoelectric Field Effect Transistor and Nanoforce Sensor Based on a Single ZnO Nanowire. *Nano Lett.* **2006**, *6*, 2768−2772.

DOI: 10.1021/acs.jpclett.5b01598
J. Phys. Chem. Lett. 2015, 6, 3410−3416

(20) Voora, V. M.; Hofmann, T.; Brandt, M.; Lorenz, M.; Grundmann, M.; Ashkenov, N.; Schmidt, H.; Ianno, N.; Schubert, M. Interface Polarization Coupling in Piezoelectric-Semiconductor Ferroelectric Heterostructures. *Phys. Rev. B: Condens. Matter Mater. Phys.* **2010**, *81*, 195307.
(21) Wu, W.; Wen, X.; Wang, Z. L. Taxel-Addressable Matrix of Vertical-Nanowire Piezotronic Transistors for Active and Adaptive Tactile Imaging. *Science* **2013**, *340*, 952−957.
(22) Wang, X.; Zhang, H.; Yu, R.; Dong, L.; Peng, D.; Zhang, A.; Zhang, Y.; Liu, H.; Pan, C.; Wang, Z. L. Dynamic Pressure Mapping of Personalized Handwriting by a Flexible Sensor Matrix Based on the Mechanoluminescence Process. *Adv. Mater.* **2015**, *27*, 2324−2331.
(23) Pan, C.; Dong, L.; Zhu, G.; Niu, S.; Yu, R.; Yang, Q.; Liu, Y.; Wang, Z. L. High-Resolution Electroluminescent Imaging of Pressure Distribution Using a Piezoelectric Nanowire LED Array. *Nat. Photonics* **2013**, *7*, 752−758.
(24) Peng, M.; Li, Z.; Liu, C.; Zheng, Q.; Shi, X.; Song, M.; Zhang, Y.; Du, S.; Zhai, J.; Wang, Z. L. High-Resolution Dynamic Pressure Sensor Array Based on Piezo-Phototronic Effect Tuned Photoluminescence Imaging. *ACS Nano* **2015**, *9*, 3143−3150.
(25) Zhang, Z.; Liao, Q.; Yu, Y.; Wang, X.; Zhang, Y. Enhanced Photoresponse of ZnO Nanorods-Based Self-Powered Photodetector by Piezotronic Interface Engineering. *Nano Energy* **2014**, *9*, 237−244.
(26) Shi, J.; Zhao, P.; Wang, X. Piezoelectric-Polarization-Enhanced Photovoltaic Performance in Depleted-Heterojunction Quantum-Dot Solar Cells. *Adv. Mater.* **2013**, *25*, 916−921.
(27) Starr, M. B.; Shi, J.; Wang, X. Piezopotential-Driven Redox Reactions at the Surface of Piezoelectric Materials. *Angew. Chem., Int. Ed.* **2012**, *51*, 5962−5966.
(28) Shi, J.; Starr, M. B.; Xiang, H.; Hara, Y.; Anderson, M. A.; Seo, J. H.; Ma, Z.; Wang, X. Interface Engineering by Piezoelectric Potential in ZnO-Based Photoelectrochemical Anode. *Nano Lett.* **2011**, *11*, 5587−5593.
(29) Shi, J.; Starr, M. B.; Wang, X. Band Structure Engineering at Heterojunction Interfaces via the Piezotronic Effect. *Adv. Mater.* **2012**, *24*, 4683−4691.
(30) Deabate, S.; Henn, F.; Devautour, S.; Giuntini, J. C. Conductivity and Dielectric Relaxation in Various Ni $(OH)_2$ Samples. *J. Electrochem. Soc.* **2003**, *150*, J23−J31.
(31) Cai, X.; Cai, Y.; Liu, Y.; Deng, S.; Wang, Y.; Wang, Y.; Djerdj, I. Photocatalytic Degradation Properties of $Ni(OH)_2$ Nanosheets/ZnO Nanorods Composites for Azo Dyes under Visible-Light Irradiation. *Ceram. Int.* **2014**, *40*, 57−65.
(32) Wang, F.; Seo, J. H.; Ma, Z.; Wang, X. Substrate-Free Self-Assembly Approach toward Large-Area Nanomembranes. *ACS Nano* **2012**, *6*, 2602−2609.
(33) Wang, F.; Jakes, J. E.; Geng, D.; Wang, X. Spontaneous Phase Transformation and Exfoliation of Rectangular Single-Crystal Zinc Hydroxy Dodecylsulfate Nanomembranes. *ACS Nano* **2013**, *7*, 6007−6016.
(34) Yan, J.; Fan, Z.; Sun, W.; Ning, G.; Wei, T.; Zhang, Q.; Zhang, R.; Zhi, L.; Wei, F. Advanced Asymmetric Supercapacitors Based on $Ni(OH)_2$/Graphene and Porous Graphene Electrodes with High Energy Density. *Adv. Funct. Mater.* **2012**, *22*, 2632−2641.
(35) Li, H. B.; Yu, M. H.; Wang, F. X.; Liu, P.; Liang, Y.; Xiao, J.; Wang, C. X.; Tong, Y. X.; Yang, G. W. Amorphous Nickel Hydroxide Nanospheres with Ultrahigh Capacitance and Energy Density as Electrochemical Pseudocapacitor Materials. *Nat. Commun.* **2013**, *4*, 1894.

DOI: 10.1021/acs.jpclett.5b01598
J. Phys. Chem. Lett. 2015, 6, 3410−3416